Ionic Glass–Gated 2D Material–Based Phototransistor: MoSe 2 over LaF 3 as Case Study

Ulrich Nguétchuissi Noumbé, Charlie Gréboval, Clément Livache, Thibault Brulé Brulé, Bernard Doudin, Abdelkarim Ouerghi, Emmanuel Lhuillier, Jean-francois Dayen

HAL Id: hal-02272351

https://hal.science/hal-02272351

Submitted on 2 Jul 2020

Ionic glass gated 2D material based phototransistor : MoSe$_2$ over LaF$_3$ as case study.

Ulrich Nguétchuissi Noumbé, Charlie Gréboval, Clément Livache, Thibault Brule, Bernard Doudin, Abdelkarim Ouerghi, Emmanuel Lhuillier*, Jean-Francois Dayen*.

U.N., Prof. B.D., Dr.J-F.D.
Université de Strasbourg, IPCMS-CMRS UMR 7504, 23 Rue du Loess, 67034 Strasbourg, France
E-mail: jean-francois.dayen@ipcms.unistra.fr

C.G., C.L., Dr. E.L.
Sorbonne Université, CNRS, Institut des NanoSciences de Paris, INSP, F-75005 Paris, France.
E-Mail : el@insp.upmc.fr

Dr.A.O.
Centre de Nanosciences et de Nanotechnologies, CNRS, Université Paris-Sud, Université Paris-Saclay, C2N–Marcoussis, 91460 Marcoussis, France

Dr. T.B.
HORIBA Scientific, HORIBA France S.A.S, Avenue de la Vauve, Passage Jobin Yvon, 91120 PALAISEAU - France

Abstract : Modulating the carrier density of two dimensional ('2D') materials is pivotal to tailor their electrical properties, with novel physical phenomena expected to occur at higher doping level. Here, the use of ionic glass as a high capacitance gate is explored to develop 2D material based phototransistor operated with higher carrier concentration up to 5×10^{13} cm^{-2}, using MoSe$_2$ over LaF$_3$ as archetypal system. Ion glass gating reveals to be a powerful technique combining the high carrier density of electrolyte gating methods while enabling direct optical addressability impeded with usual electrolyte technology.

The phototransistor demonstrates I$_{ON}$/I$_{OFF}$ ratio exceeding 5 decades and photoresponse times down to 200 µs, up to two decades faster than MoSe$_2$ phototransistors reported so far. Carefull phototransport analysis unveils that ionic glass gating of 2D materials allows tuning the nature of the carrier recombination processes, while annihilating completely the traps

1

contribution in electron injection regime. This remarkable property results in photoresponse that can be modulated electrostatically by more than two orders of magnitude, while at the same time increasing the gain bandwidth product. This study demonstrates the potential of ionic glass gating to explore novel photoconduction processes and alternative architectures of devices.

1. Introduction

Because they combine a band gap with new optical features[1] resulting from their low dimensionality Transition Metal DiChalcogenides (TMDC) are generating a lot of interests to revisit the 2D physics of semiconductor.[2–4] The control of carrier density becomes of utmost importance to design building block such as pn junction[5,6], field effect transistor (FET) [7], light emitting diode[8] and photodetector[3,9,10]. Due to chalcogenides vacancy TMDC are not behaving as intrinsic semiconductor, $MoSe_2$ is n type while WSe_2 is p type for example. Post synthesis control of this doping is also possible thanks to hydrogenation,[11] deposition of small electron donor and acceptor molecule.[12,13] All these methods however still suffer from a lack of post fabrication tunability, and may require alternative device fabrication process such as resist free patterning[14,15]. Gate control of the carrier density remains the most conventional method to tune the carrier density at the device level.[16] Two main strategies have been proposed to gate 2D material which are conventional dielectric (typically the silica layer on the top of a silicon wafer) and electrolyte (ionic liquid, ion gel…). In the first approach, dielectric breakdown limits the maximum accumulated carrier density within the 10^{12} cm^{-2} range. The second method is of utmost interest when larger sheet density ($>10^{13}$ cm^{-2}) are targeted.[17–19] Use of electrolyte has been exploited in TMDC to develop ambipolar FET[20], to induce superconductivity[21] or for the design of pn junction.[22–24] An important drawback of electrolyte gate technology, is that the electrolyte covers the gated material, hindering direct

top optical excitation since it can absorb or scatter the light, and preventing its use for optoelectronics devices and optical studies.

Some alternative to dielectric and electrolyte have been proposed and rely on ferroelectric polymer[25] and more recently on the use of ionic glasses. The Shukla's group[22] has proposed to use borosilicate and soda-lime glasses as ionic glass media. By applying a large electric field on such glass slide at high temperature (400 K), ions within the glass substrate can accumulate at the sample surface leading to a gate effect. While the method can be used to reach high carrier density above 10^{14} cm^{-2}, the gate effect can only be obtained far above room temperature. The Cui's group[28] later proposed to change these glass for LaF_3 and demonstrated gate effect under dark condition on MoS_2, while preserving the gate tunability down to 180K circumventing the need for large electric field and high temperature imposed by borosilicate and soda-lime glasses. However, there is no report to date on the use of ionic glass for photodetection. Here, we explore for the first time the possibility to control the photoresponse of a 2D material over an extended doping range with ion glass gating, using $MoSe_2$ flakes over LaF_3 ionic glass as archetypal system. Our $MoSe_2$/Ionic Glass phototransistor demonstrate high and fast photoresponsivity respect to the state of the art. Moreover, we demonstrate that ionic glass gating can be used as a knob to tune the nature of the carrier recombination processes, while annihilating completely the traps contribution in electron injection regime. This new functionality enables to modulate electrostatically the magnitude of the photoresponse over more than two orders of magnitude. Surprisingly, this change is achieved while preserving the photoresponse time, i.e, while amplifying the gain bandwidth product.

2. Results and discussion

We first start by preparing a MoSe$_2$ flake using exfoliation method and transfer it onto the LaF$_3$ substrate. Few layers MoSe$_2$ flake was mechanically exfoliated from bulk crystal on Polydimethylsiloxane (PDMS) using adhesive tapes, and then transferred onto LaF$_3$ substrate by dry transfer method[29]. The optical transparency of the LaF$_3$ substrate allows for simple identification of the flakes by optical contrast. The lack of PL signal suggests that the flake is made of multilayers MoSe$_2$.[30] This hypothesis is further confirmed by the Raman map and spectrum, see **Figure 1.c** and **Figure 1.d**. The A1g peak of MoSe$_2$ here appears at 242 cm^{-1}, while it is expected to be at 240 cm^{-1} for the monolayer MoSe$_2$, confirming the multilayer aspect of our sample. Finally using Atomic Force Microscopy, we determine the thickness of the sample to be 2.5±0.5 nm, which correspond to 4-5 monolayers of MoSe$_2$.

The flake is then connected to gold electrodes by electron beam lithography using a standard bilayer PMMA (Polymethyl methacrylate) resist and an additional conductive Protective Coating resist. A scheme of the phototransistor device as well as scanning electron microscopy image are given in **Figure 1.a-b**. Finally, the sample is inserted into a cryostat for temperature dependent phototransport study.

As gate bias is applied, F$^-$ vacancy moves toward or away from the surface which induce electrostatic gating effect[28]. The MoSe$_2$ flake presents a n-type characteristic which is consistent with previous MoSe$_2$ based FET using SiO$_2$ as dielectric,[31,32] see **Figure 2a-b**. It is important to note that field effect is preserved even for operation below room temperature. Actually we observe a maximum of the current modulation for a device temperature around 200 K, see **Figure 2c**. There the I$_{ON}$/I$_{OFF}$ current modulation exceeds 5 orders of magnitude (I$_{on}$/I$_{off}$=2x10^5 for V$_{DS}$=0.5 V), see **Figure 2b-c**. Above 200 K, the On-off ratio is limited by a large off current due to the relatively large leakage through the LaF$_3$. At temperature below

180K, the ionic mobility of the F^- vacancy gets strongly reduced and the ON current gets lower, see **Figure 2c**. A subthreshold slope, defined as $S=(d(logI_{DS})/dV_{GS})^{-1}$ of S≈240 mV/decade can be extracted at V_{DS}=1V.

To have a deeper insight into the ionic glass gating mechanisms, the capacitance of LaF_3 as a function of frequency (C(f)) has been determined using an impedance meter, see Inset of **Figure 2d** (see also Supporting Information and **Figure S1** for technical details). At high frequency the capacitance of the substrate is weak. At such high frequency, ions do not have enough time to reach the surface, only the dielectric behavior of the substrate is observed. Because the LaF_3 substrate is quite thick (>1 mm), its capacitance is weak. At lower frequency, ions get enough time to reach the surface and can form the equivalent of a ionic double layer, and a significant rise of the capacitance is observed which now reach 1 $\mu F.cm^{-2}$, a value quite similar to those reported for electrolytes[17]. Such large capacitance allows low gate bias operability, typically around a few volts, since carrier concentration as large as $5x10^{13}$ cm^{-2} are achieved under 8 V operation.

Using the C(f) curve it is now possible to estimate the field effect electronic mobility using the expression $\mu_{FE} = \frac{L}{wC_\Sigma V_{DS}}\frac{\partial I_{DS}}{\partial V_{GS}}$, where L is the electrode spacing (2.6 µm), W is the electrode length (9.3 µm), C_Σ the surface capacitance taken equal to 0.1 $\mu F.cm^{-2}$ at 200K (see inset of **Figure 2d**). We found electron mobility to be μ_{FE}≈ 15 $cm^2 \cdot V^{-1} \cdot s^{-1}$ at 200 K, see **Figure 2d**. This value is very similar to the one reported for $MoSe_2$ multilayer gated with silica.[32]

While for TMDC the concept of dark current control using LaF_3 has already been reported[28], we here extend this concept and demonstrate for the first time that the photoresponse of 2D semiconducting material can also be tuned thanks to the ionic glass gate (see Supporting Information and **Figure S2** for technical details). Under illumination above

the band gap (by a 405 nm blue laser), we observe a photoconductive signal, see **Figure 3a**.

The magnitude of the signal can be strongly tuned using the gate bias, see **Figure 3b**.

Typically, the responsivity of the film reaches 50 mA/W at 0 V of gate bias and is enhanced

by a factor 4 under strong positive gate bias now exceeding 0.2 A/W. It is worth pointing that

the increase of the responsivity is not as fast as the one of the dark current. As a result the gate

bias which maximizes the signal to noise ratio is obtained under hole injection, see **Figure 3d**.

This regime corresponds to the one which minimizes the dark current. Rise- and fall-times

(respectively t_{ON} and t_{OFF} in **Figure 3.c**) extracted from the photocurrent characteristics under

negative gate bias are close to 200 µs and 600 µs respectively. This is two orders of

magnitude faster than time responses previously reported on usual exfoliated and CVD $MoSe_2$

[10,33–37], 50 times faster than encapsulated $MoSe_2$ devices[38], and more than one decade shorter

than the fastest $MoSe_2$ phototransistor reported so far[39]. Another very striking feature comes

from the very weak gate dependence of the time response with gate bias, see **Figure 3c**. The

on and off time change by less than 30 % from the hole injection to the electron injection

regimes. This is remarkable since the gain bandwidth product (which can be seen as the ratio

of responsivity divided by the characteristic time constant) is actually increasing with the

applied gate. This result contrast with what is observed for phototransistor based on

nanocrystal film, [40,41] where the change of responsivity is made at quasi constant gain

bandwidth product. In other words, a higher photoresponse comes at the prize of a slower

response, on the contrary of our device.

We have then used the power dependence of the photoresponse to reveal the

recombination mechanism. While the incident power is increased, the photocurrent rises, see

Figure 4a-b. However this increase presents a sub-linear dependence and appears to be gate

tunable, see **Figure 4b**. Under electron injection (ie positive gate bias) the current as a

function of incident power follows a power law with an exponent of 0.42, which is quite close

to the value of ½ expected for bimolecular process[42,43] (*ie* recombination occurs through electron hole recombination). On the other hand, under hole injection we observe an increase of the exponent value which now reached 0.67. This value is typically intermediate between the value of ½ expected for bimolecular process and the value of 1 obtained for monomolecular process (ie for trapping). By applying a negative gate bias the Fermi level is brought more deeply in the band gap and the recombination centers get unfilled and can act as trap states, which explain the increase of the power law exponent, see the associated mechanism in the inset of **Figure 4b**.

3. Conclusion

We have explored the potential of LaF_3 ionic glass to build TMDC based phototransistor with low operating bias and preserving gate tunability down to 180 K. Optimal operating temperature is around 200K and limits the leakage through the substrate while preserving a strong ionic mobility, with I_{ON}/I_{OFF} ratio exceeding 5 decades. Not only the dark conductance can be tuned but also the photoresponse which demonstrates time responses down to 200 µs, up to two decades faster than state of the art $MoSe_2$ phototransistors reported so far. Careful analysis of photocurrent properties reveals that the relative contribution of traps on the carrier recombination can be dramatically suppressed thanks to the very high accumulated carrier concentration achieved by ion glass gating. In other words, the ion glass gate can be used as knob to switch on and off monomolecular recombination processes. Remarkably, this novel functionality allows for modulating the device photoresponse by more than two orders of magnitude, while at the same time increasing its gain bandwidth product, a unique property never observed on any other nanomaterials such as nanocrystals.

This study shows that ionic glass gate are complementary method to the usual electrolyte gate approaches, as they enable optical experiments in high doping regime that are not

possible when the 2D material is buried into the electrolyte gate. The performances of our ionic glass photodetector demonstrate the potential of this method to explore novel photoconduction processes and alternative architectures of devices. Our approach is generic, and can be easily extended to any photoconducting nanomaterials, including organic and molecular systems[44–46], nanocrystals[47,48], and hybrid materials[49–54].

4. Experimental section

Device fabrication : Few layer $MoSe_2$ was mechanically exfoliated from bulk crystal (2H phase from graphene supermarket) on PDMS (Polydimethylsiloxane) using adhesive tapes, and then transferred onto LaF_3 substrate by dry transfer method [29]. By optical contrast, we identified the flake and, we used Ebeam lithography with a Zeiss Supra 40 scanning electron microscope coupled to a Raith lithography system to pattern electrodes. We used a standard bilayer PMMA (Polymethyl methacrylate) resist and a conductive Protective Coating resist (e-spacer) to write on the insulator surface. The PMMA bilayer consists of AR-PMMA 669.04 and AR-PMMA 679.02, that were spin-coated at 4000 revolutions per minute (rpm) during 1 min and annealed at 180 °C during 90 seconds (220nm / 4000rpm and 70nm / 4000rpm respectively). The e-spacer AR-PC 5090.02 was then spincoated at the same speed (4000 rpm) but annealed at 90 °C during 90 seconds (90nm /4000rpm). After the development in 1:3 MIBK-IPA at 25 °C, metal deposition Ti(3nm)/Au(47nm) was performed by electron beam evaporator in high vacuum chamber, followed by lift-off in acetone, rinsing with isopropanol and nitrogen jet drying.

Scanning electron microscopy : SEM is made using a FEI Magellan microscope. Images are acquired with the e-beam accelerated with a 3 kV bias and the current from the electronic gun set at 6 pA.

Raman and photoluminescence spectra : The micro-Raman and photoluminescence (PL) measurements were conducted using commercial confocal HORIBA LabRAM HR Evolution

micro-Raman microscope with an objective focused 532 nm and 633 nm lasers in an ambient environment at room temperature. The excitation laser was focused onto the samples with a spot diameter of ≈0.5 µm and incident power of ≈0.1 mW. Measurements were performed on the same microscope with a 100× objective and a CCD detector (detection range from 1.2 to 6.2 eV).

Photocurrent and electrical measurements : The sample is connected to a Keithley K2634 B in a cryostat. It controls the applied gate voltage (V_{GS}) and the applied drain-source bias (V_{DS}). The sample is illuminated by a 405 nm laser chopper at 100 Hz. A transimpedance amplifier DLPCA-200 is added to the circuit to measure the photocurrent on a GHz oscilloscope. See supporting information for more details, and **Figure S2**.

Capacitance measurements: To measure the capacitance of the sample, 80 nm of Au is evaporated on both sides of the LaF_3 substrate. It is then connected to a MFLI lock-in amplifier that applies an AC bias of 300 mV and measures the current. See supporting information for more details, and **Figure S1**.

Supporting Information

Supporting Information is available from the Wiley Online Library or from the author.

Acknowledgments

References

[1] K.F. Mak, C. Lee, J. Hone, J. Shan, and T.F. Heinz, Phys. Rev. Lett. **105**, 136805 (2010).

[2] S. Manzeli, D. Ovchinnikov, D. Pasquier, O. V. Yazyev, and A. Kis, Nat. Rev. Mater. **2**, natrevmats201733 (2017).

[3] M. Long, P. Wang, H. Fang, and W. Hu, Adv. Funct. Mater. 1803807 (2018).

[4] X. Duan, C. Wang, A. Pan, R. Yu, and X. Duan, Chem. Soc. Rev. **44**, 8859 (2015).

[5] M.S. Choi, D. Qu, D. Lee, X. Liu, K. Watanabe, T. Taniguchi, and W.J. Yoo, ACS Nano **8**, 9332 (2014).

[6] L. Lin, L. Liao, J. Yin, H. Peng, and Z. Liu, Nano Today **10**, 701 (2015).

[7] B. Radisavljevic, A. Radenovic, J. Brivio, V. Giacometti, and A. Kis, Nat. Nanotechnol. **6**, 147 (2011).

[8] W. Zheng, Y. Jiang, X. Hu, H. Li, Z. Zeng, X. Wang, and A. Pan, Adv. Opt. Mater. **6**, 1800420 (2018).

[9] O. Lopez-Sanchez, D. Lembke, M. Kayci, A. Radenovic, and A. Kis, Nat. Nanotechnol. **8**, 497 (2013).

[10] C. Xie, C. Mak, X. Tao, and F. Yan, Adv. Funct. Mater. **27**, 1603886 (2017).

[11] M.G. Silly, F. Bertran, D. Pierucci, J.E. Rault, A. Ouerghi, P. Le Fèvre, A.T.C. Johnson, H. Henck, F. Sirotti, C.H. Naylor, A. Balan, Y.J. Dappe, and Z. Ben Aziza, ACS Nano **11**, 1755 (2017).

[12] J. Wang, Z. Ji, G. Yang, X. Chuai, F. Liu, Z. Zhou, C. Lu, W. Wei, X. Shi, J. Niu, L. Wang,

H. Wang, J. Chen, N. Lu, C. Jiang, L. Li, and M. Liu, Adv. Funct. Mater. **28**, 1806244 (2018).

[13] S. Mouri, Y. Miyauchi, and K. Matsuda, Nano Lett. **13**, 5944 (2013).

[14] H.-C. Cheng, R.-J. Shiue, C.-C. Tsai, W.-H. Wang, and Y.-T. Chen, ACS Nano **5**, 2051 (2011).

[15] A. Mahmood, C.-S. Yang, J.-F. Dayen, S. Park, M.V. Kamalakar, D. Metten, S. Berciaud, J.-O. Lee, and B. Doudin, Carbon N. Y. **86**, 256 (2015).

[16] Z.M. Wang, X. Tong, E. Ashalley, F. Lin, and H. Li, Nano-Micro Lett. **7**, 203 (2015).

[17] J. Lee, M.J. Panzer, Y. He, T.P. Lodge, and C.D. Frisbie, J. Am. Chem. Soc. **129**, 4532 (2007).

[18] J. Ye, M.F. Craciun, M. Koshino, S. Russo, S. Inoue, H. Yuan, H. Shimotani, A.F. Morpurgo, and Y. Iwasa, Proc. Natl. Acad. Sci. U. S. A. **108**, 13002 (2011).

[19] H.T. Yuan, M. Toh, K. Morimoto, W. Tan, F. Wei, H. Shimotani, C. Kloc, and Y. Iwasa, Appl. Phys. Lett. **98**, 012102 (2011).

[20] Y. Zhang, J. Ye, Y. Matsuhashi, and Y. Iwasa, Nano Lett. **12**, 1136 (2012).

[21] J.T. Ye, Y.J. Zhang, R. Akashi, M.S. Bahramy, R. Arita, and Y. Iwasa, Science **338**, 1193 (2012).

[22] Y.J. Zhang, J.T. Ye, Y. Yomogida, T. Takenobu, and Y. Iwasa, Nano Lett. **13**, 3023 (2013).

[23] H. Xu, S. Fathipour, E.W. Kinder, A.C. Seabaugh, and S.K. Fullerton-Shirey, ACS Nano **9**, 4900 (2015).

[24] H. Henck, D. Pierucci, J. Chaste, C.H. Naylor, J. Avila, A. Balan, M.G. Silly, M.C. Asensio, F. Sirotti, A.T.C. Johnson, E. Lhuillier, and A. Ouerghi, Appl. Phys. Lett. **109**, 113103 (2016).

[25] Y. Zheng, G.-X. Ni, C.-T. Toh, C.-Y. Tan, K. Yao, and B. Özyilmaz, Phys. Rev. Lett. **105**, 166602 (2010).

[26] J. Biscaras, Z. Chen, A. Paradisi, and A. Shukla, Nat. Commun. **6**, 8826 (2015).

[27] A. Paradisi, J. Biscaras, and A. Shukla, Appl. Phys. Lett. **107**, 143103 (2015).

[28] C.L. Wu, H. Yuan, Y. Li, Y. Gong, H.Y. Hwang, and Y. Cui, Nano Lett. **18**, 2387 (2018).

[29] A. Castellanos-Gomez, M. Buscema, R. Molenaar, V. Singh, L. Janssen, H.S.J. van der Zant, and G.A. Steele, 2D Mater. **1**, 011002 (2014).

[30] X. Zhang, D.R.T. Zahn, J. Börner, M. Albrecht, O. Gordan, S. Michaelis de Vasconcellos, C. Kloc, P. Tonndorf, P. Böttger, R. Bratschitsch, A. Liebig, and R. Schmidt, Opt. Express **21**, 4908 (2013).

[31] S. Larentis, B. Fallahazad, and E. Tutuc, Appl. Phys. Lett. **101**, 223104 (2012).

[32] L.D.N. Mouafo, F. Godel, G. Froehlicher, S. Berciaud, B. Doudin, M.V. Kamalakar, and J.-F. Dayen, 2D Mater. **4**, 015037 (2016).

[33] A. Abderrahmane, P.J. Ko, T. V Thu, S. Ishizawa, T. Takamura, and A. Sandhu, Nanotechnology **25**, 365202 (2014).

[34] T. Dai, Y. Liu, X. Liu, D. Xie, and Y. Li, J. Alloys Compd. **785**, 951 (2019).

[35] Y.-H. Chang, W. Zhang, Y. Zhu, Y. Han, J. Pu, J.-K. Chang, W.-T. Hsu, J.-K. Huang, C.-L. Hsu, M.-H. Chiu, T. Takenobu, H. Li, C.-I. Wu, W.-H. Chang, A.T.S. Wee, and L.-J. Li, ACS Nano **8**, 8582 (2014).

[36] J. Xia, X. Huang, L.-Z. Liu, M. Wang, L. Wang, B. Huang, D.-D. Zhu, J.-J. Li, C.-Z. Gu, and X.-M. Meng, Nanoscale **6**, 8949 (2014).

[37] C. Jung, S.M. Kim, H. Moon, G. Han, J. Kwon, Y.K. Hong, I. Omkaram, Y. Yoon, S. Kim, and J. Park, Sci. Rep. **5**, 15313 (2015).

[38] D. Kufer and G. Konstantatos, Nano Lett. **15**, 7307 (2015).

[39] H. Lee, J. Ahn, S. Im, J. Kim, and W. Choi, Sci. Rep. **8**, 11545 (2018).

[40] H. Aubin, B. Dubertret, E. Lhuillier, S. Ithurria, and A. Robin, Nano Lett. **14**, 2715 (2014).

[41] C. Livache, E. Izquierdo, B. Martinez, M. Dufour, D. Pierucci, S. Keuleyan, H. Cruguel, L. Becerra, J.L. Fave, H. Aubin, A. Ouerghi, E. Lacaze, M.G. Silly, B. Dubertret, S. Ithurria, and E. Lhuillier, Nano Lett. **17**, 4067 (2017).

[42] A. Rose, *Concepts in Photoconductivity and Allied Problems* (Interscience Publishers, 1963).

[43] L.J. Willis, J.A. Fairfield, T. Dadosh, M.D. Fischbein, and M. Drndic, Nano Lett. **9**, 4191 (2009).

[44] K.-J. Baeg, M. Binda, D. Natali, M. Caironi, and Y.-Y. Noh, Adv. Mater. **25**, 4267 (2013).

[45] F. Yang, S. Cheng, X. Zhang, X. Ren, R. Li, H. Dong, and W. Hu, Adv. Mater. **30**, 1702415 (2018).

[46] S. Zanettini, J.F. Dayen, C. Etrillard, N. Leclerc, M.V. Kamalakar, and B. Doudin, Appl. Phys. Lett. **106**, 063303 (2015).

[47] E. Lhuillier, S. Pedetti, S. Ithurria, B. Nadal, H. Heuclin, and B. Dubertret, Acc. Chem. Res. **48**, 22 (2015).

[48] E. Lhuillier, J.F. Dayen, D.O. Thomas, A. Robin, B. Doudin, and B. Dubertret, Nano Lett. **15**, 1736 (2015).

[49] S. Parui, L. Pietrobon, D. Ciudad, S. Vélez, X. Sun, F. Casanova, P. Stoliar, and L.E. Hueso, Adv. Funct. Mater. **25**, 2972 (2015).

[50] C. Gong, K. Hu, X. Wang, P. Wangyang, C. Yan, J. Chu, M. Liao, L. Dai, T. Zhai, C. Wang, L. Li, and J. Xiong, Adv. Funct. Mater. **28**, 1706559 (2018).

[51] D. Jariwala, T.J. Marks, and M.C. Hersam, Nat. Mater. **16**, 170 (2017).

[52] F. Godel, L.D.N. Mouafo, G. Froehlicher, B. Doudin, S. Berciaud, Y. Henry, J.-F. Dayen, D. Halley, L.D.N.M. Florian Godel, F. Godel, L.D.N. Mouafo, G. Froehlicher, B. Doudin, S. Berciaud, Y. Henry, J.-F. Dayen, and D. Halley, Adv. Mater. **29**, 1604837 (2017).

[53] L.D.N. Mouafo, F. Godel, G. Melinte, S. Hajjar-Garreau, H. Majjad, B. Dlubak, O. Ersen, B. Doudin, L. Simon, P. Seneor, and J.-F. Dayen, Adv. Mater. 1802478 (2018).

[54] W. Zheng, B. Zheng, C. Yan, Y. Liu, X. Sun, Z. Qi, T. Yang, Y. Jiang, W. Huang, P. Fan, F. Jiang, W. Ji, X. Wang, and A. Pan, Adv. Sci. 1802204 (2019).
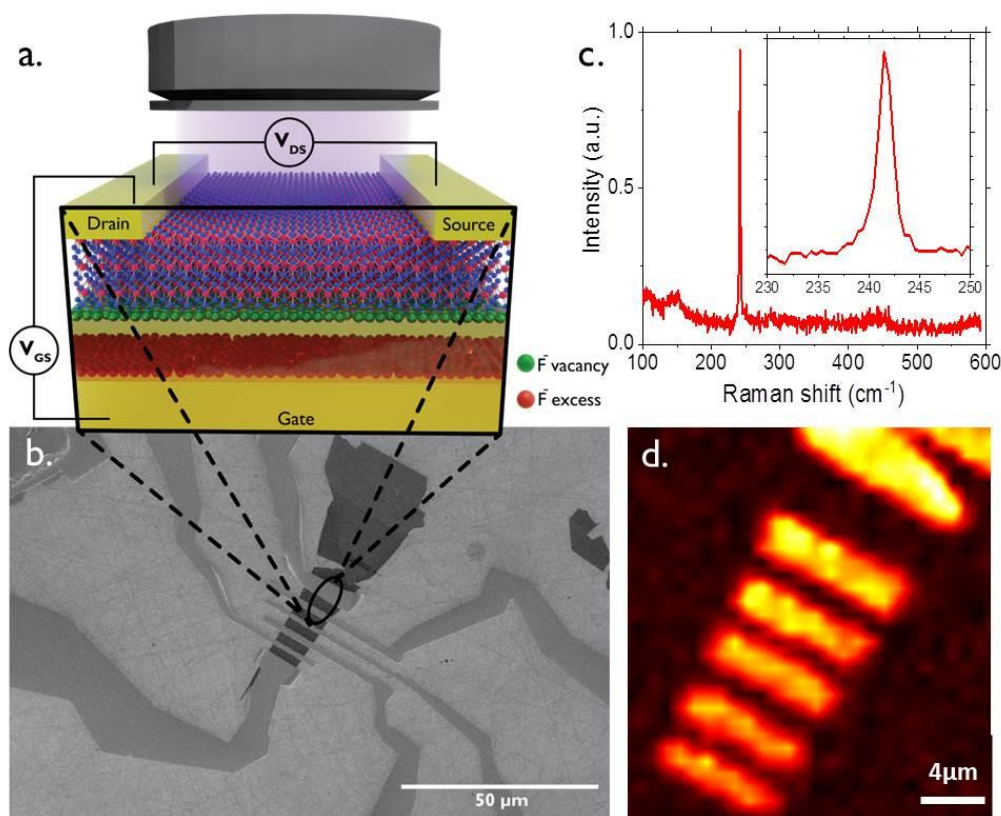
Figure 1. a) Scheme of the photodetector device and electrical connections. A flake of $MoSe_2$ on a LaF_3 substrate is contacted by 2 gold electrodes (Drain and Source) and gating is performed by applying a bias between drain and a bottom gold contact below LaF_3. Top access allows addressing optically the $MoSe_2$ channel while reaching higher carrier density thanks to the ionic glass gate. b) SEM image of the flake and gold contacts. Length and width of the channel are respectively 2.6 and 9.3 µm. c) Raman spectrum of the $MoSe_2$ flake. The inset is a zoom on the peak relative to the A1g mode of $MoSe_2$.(d) Raman map around the $MoSe_2$ flake contacted by the gold electrodes.
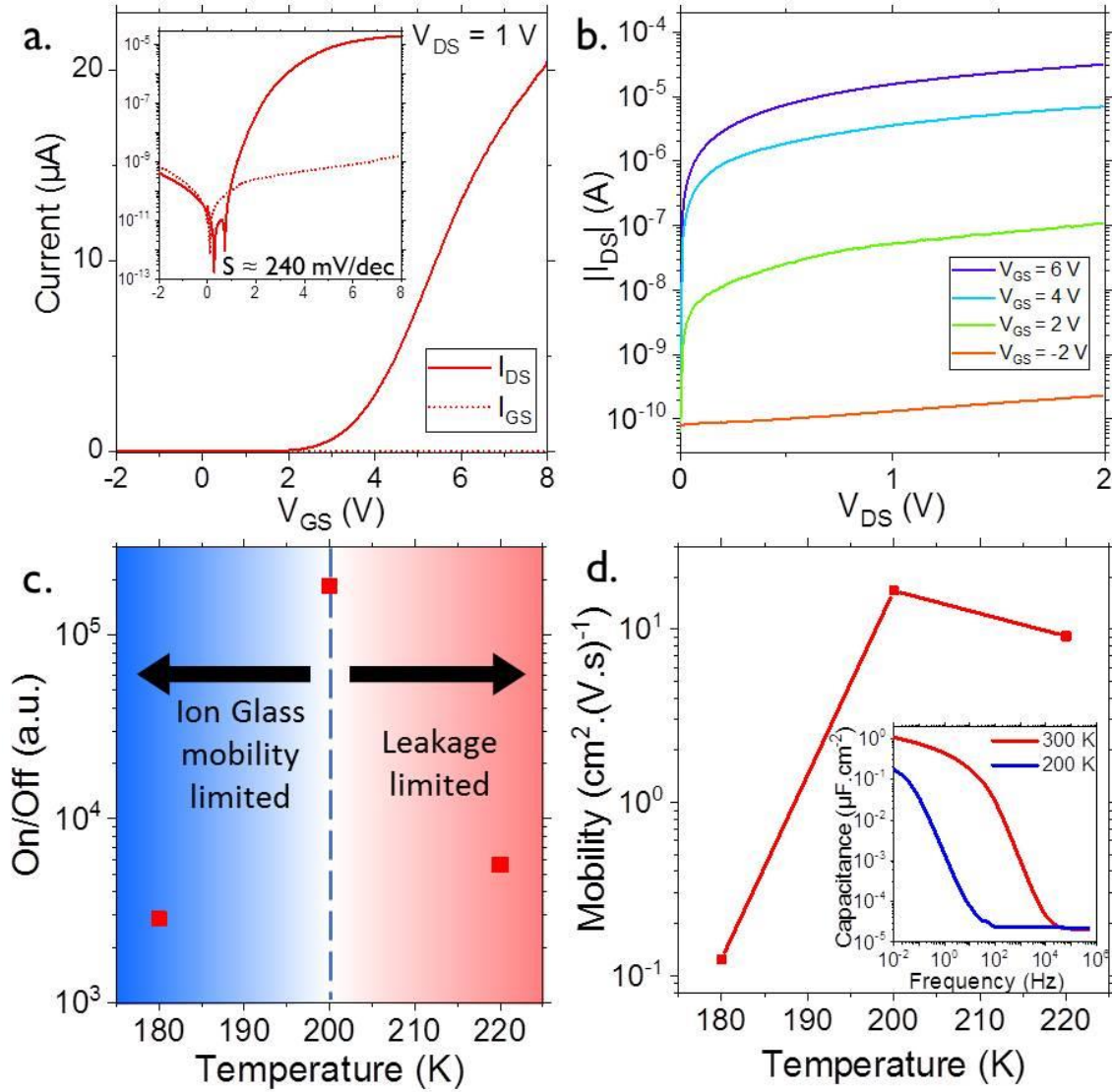
Figure 2. a) Transfer curve of an MoSe$_2$ flake under 1 V drain-source bias at 200 K in linear scale. Inset: Transfer curve in logarithmic scale. b) IV curves at different gate biases measured at 200 K. c) On/Off ratios calculated from transfer curves at V$_{DS}$ = 1V. d) Electrical mobility calculated from transfer curves at different temperatures assuming a capacitance of 0.1 µF.cm^{-2}. Inset: Capacitance measured at different frequencies on a 1 mm thick LaF$_3$ substrate providing insight into the ion glass gating mechanisms.
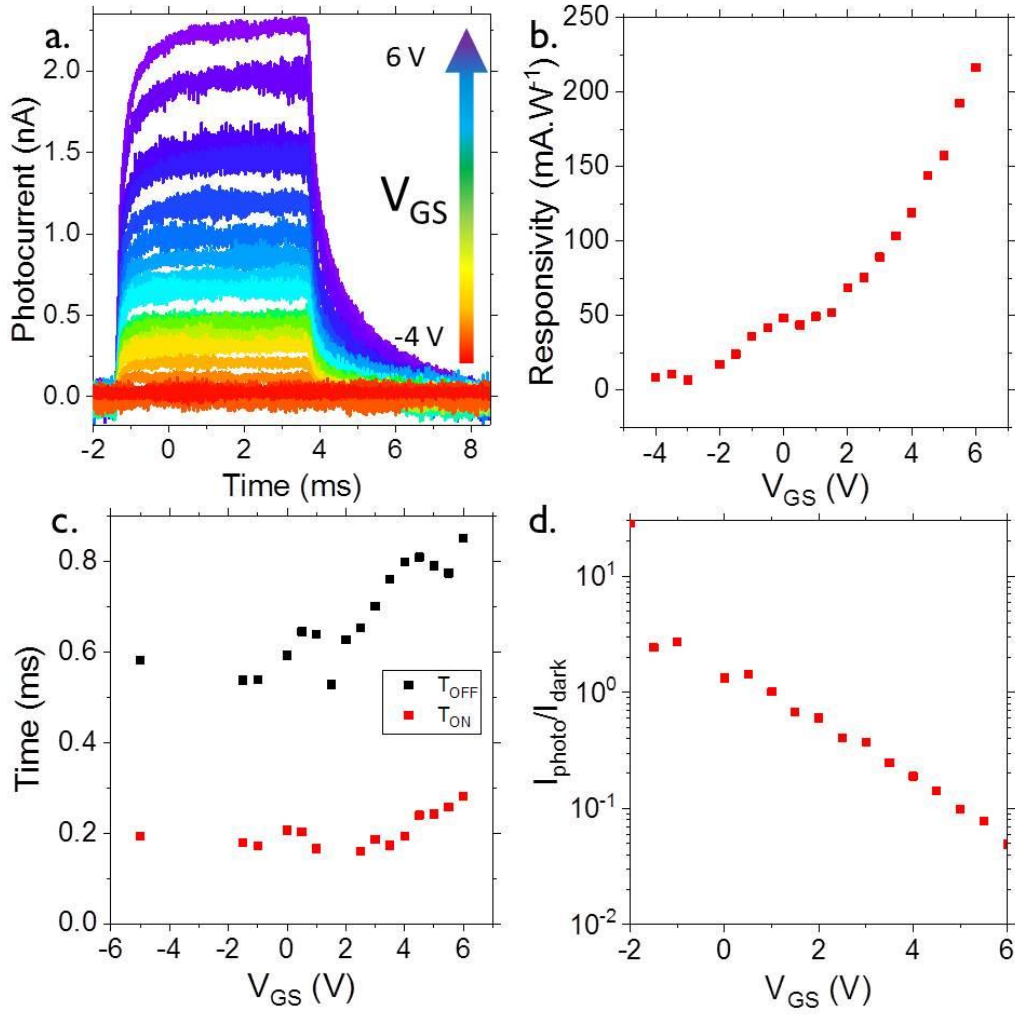
Figure 3. a) Photocurrent of the device illuminated under 12 nW received power from a 405 nm laser chopped at 100 Hz and 180 K at different voltages. Drain-source bias is 1 V. b) Responsivity of the device under different gate voltages calculated with the power received by the device at 100 Hz and 180 K. c) Rise- and fall-times extracted from (a) using a single exponential fit at different gate voltages. d) Photocurrent over dark-current at 100 Hz and 180 K for different gate voltages under 1 V drain-source bias.
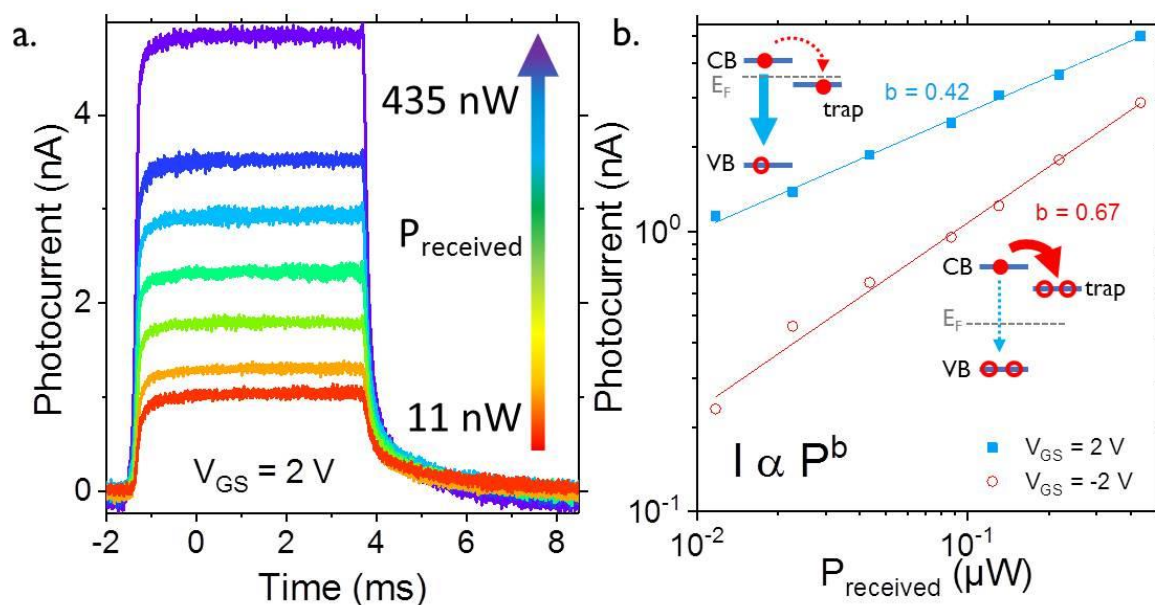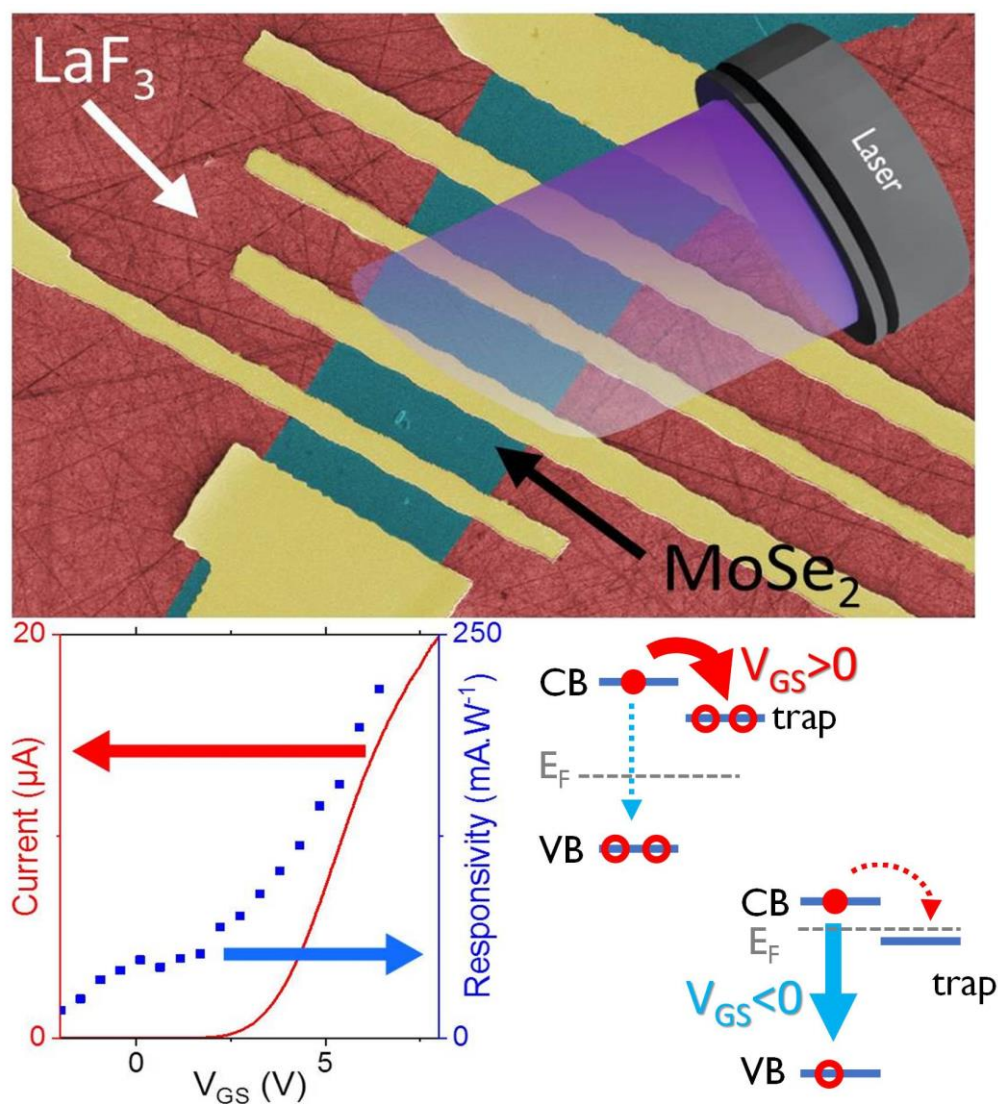
Figure 4. a) Photocurrent at 100 Hz and 180 K for different incident power (from 11 nW to 435 nW) under 2 V of gate bias. b) Power dependency of the photocurrent at 100 Hz and 180 K under two gate voltages. Power law fit of the data points. Schemes as inset illustrate the relaxation mechanism associated with each curves(bimolecular process is represented by the blue arrow, monomolecular process by the red arrow).

Keyword : optoelectronics

Ulrich Noumbe, Charlie Gréboval, Clément Livache, Thibault Brule, Bernard Doudin, Abdelkarim Ouerghi, Emmanuel Lhuillier*, Jean-Francois Dayen*.

Ionic glass gated 2D material based phototransistor : MoSe$_2$ over LaF$_3$ as case study.

TOC text : We report for the first time 2D material based photodetector using ionic glass as electrostatic gating method, choosing MoSe$_2$ over LaF$_3$ ionic glass as archetypal system. We unveil the wider possibilities offered by this architecture, and provide a careful analysis of its unique optoelectronic properties.

Supporting Information

Ionic glass gated 2D material based phototransistor : MoSe$_2$ over LaF$_3$ as case study.

Ulrich Nguétchuissi Noumbé, Charlie Gréboval, Clément Livache, Thibault Brule, Bernard Doudin, Abdelkarim Ouerghi, Emmanuel Lhuillier*, Jean-Francois Dayen*.

To whom correspondence should be sent:
el@insp.upmc.fr , jean-francois.dayen@ipcms.unistra.fr

1. AFM measurements

The thickness of the sample was revealed using Atomic Force Microscoscopy. It is found to be 2.5±0.5 nm, which correspond to 4-5 monolayers of MoSe$_2$.
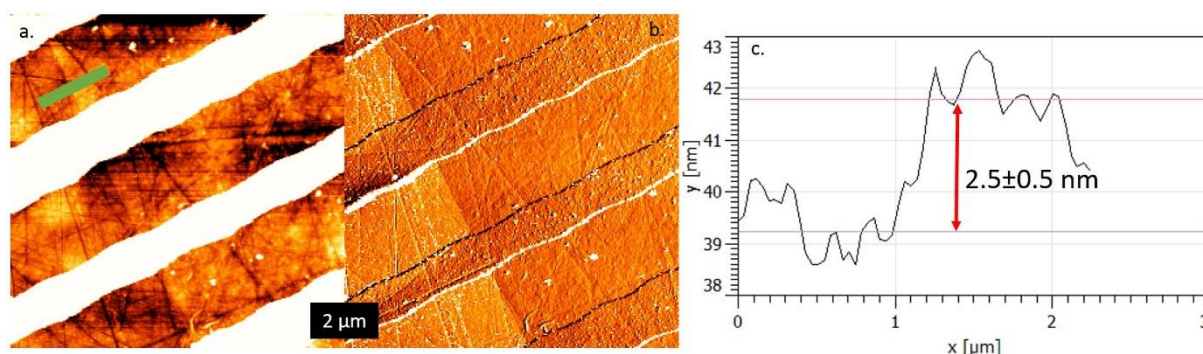

Figure S 1 Magnitude (a.) and phase (b.) atomic force microscopy image of the MoSe$_2$ flake. The white line in the magnitude image results from the gold contact. C. height profile corresponding to the green line in part a.

2. Impedance measurements

To measure the capacitance of the sample, 80 nm of Au is evaporated on both sides of the

LaF$_3$ substrate. It is then connected to a MFLI lock-in amplifier that applies an AC bias of 300

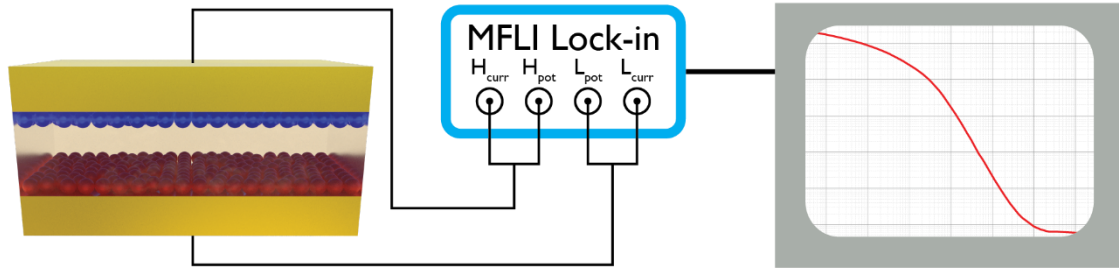mV and measures the current, as scheme of the setup is shown in **Figure S1**.

Figure S1. Experimental setup for capacitance measurements. Gold is evaporated on both sides of the substrate. The contacts are made with silver paste. A lock-in amplifier is used to apply an AC voltage at a given frequency. The lock-in then measures the current through the sample in order to calculate the capacitance.

3. Photocurrent measurement

The sample is illuminated by a 405 nm laser chopper at 100 Hz. The sample is connected to a

Keithley K2634 B in a cryostat. It controls the applied gate voltage (V_{GS}) and the applied

drain-source bias (V_{DS}). A transimpedance amplifier DLPCA-200 is added to the circuit to

measure the photocurrent on a GHz oscilloscope, as depicted in **Figure S2**.
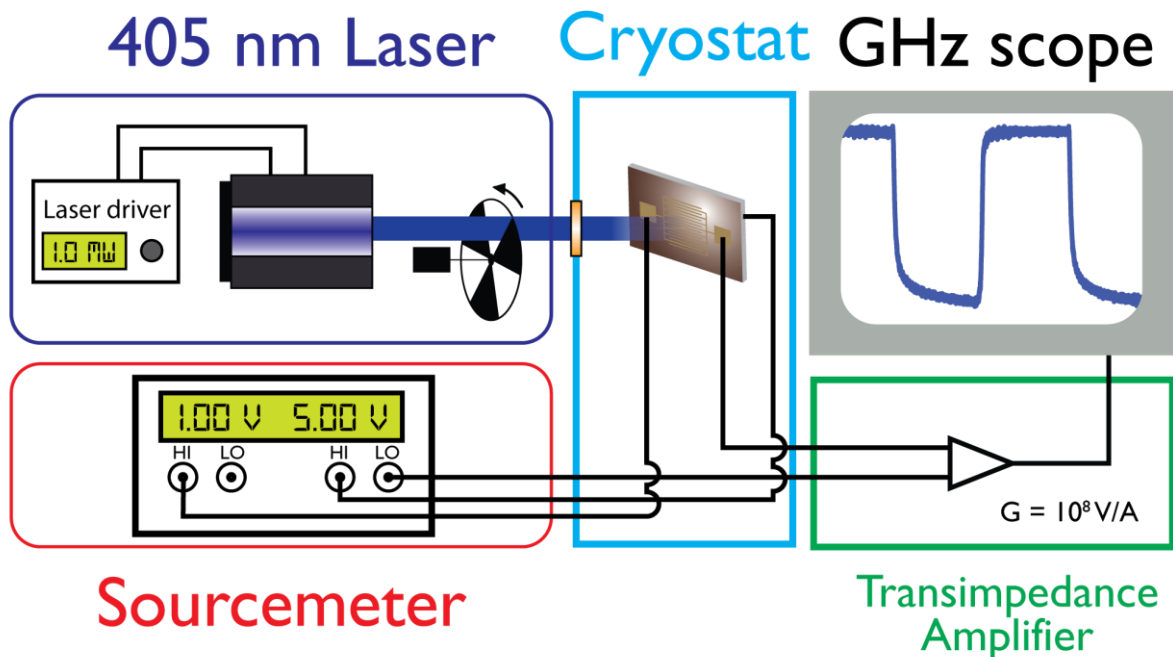

Figure S2. Experimental setup for photocurrent measurement. A 405 nm laser is chopped at 100 Hz and illuminates the sample in the cryostat. Sample is biased by a Keithley 2634 B and a DLPCA-200 transimpedance amplifier is connected to a GHz oscilloscope. A gate bias is applied using a Keithley 2634 B.